Supporting Information

Energy absorption characteristics of additively manufactured plate-lattices under low-velocity impact loading

Jefferson Andrew J[a], Johannes Schneider[a,b], Jabir Ubaid[a], R Velmurugan[c], N K Gupta[d], S Kumar[a,b,*]

[a]Department of Mechanical Engineering, Khalifa University of Science and Technology, Masdar Campus, Masdar City, P.O. Box 54224, Abu Dhabi, UAE.

[b]James Watt School of Engineering, University of Glasgow, Glasgow G12 8LT, UK.

[c]Department of Applied Mechanics, Indian Institute of Technology Delhi, New Delhi 110016, India.

[d]Department of Aerospace Engineering, Indian Institute of Technology Madras, Chennai 600036, India

*Corresponding author: s.kumar@eng.oxon.org

S1. Modeling, fabrication and testing

S1.1. Estimation of volume fraction of elementary plate-lattices in the hybrid structures

There are three topological constraints that guarantee isotropic elastic response of a hybrid plate lattice structure if satisfied [1] at the macroscopic level.

$$\sum_{\alpha \in UC} c^{(\alpha)} \left(n_k{}^{(\alpha)}\right)^2 n_l{}^{(\alpha)} n_m{}^{(\alpha)} = 0 \qquad \text{for } k,l,m = 1,..,3 \text{ with } l \neq m \tag{1}$$

$$\sum_{\alpha \in UC} c^{(\alpha)} \left(n_k{}^{(\alpha)}\right)^4 = \frac{\rho^*}{5} \qquad \text{for } k = 1,..,3 \tag{2}$$

$$\sum_{\alpha \in UC} c^{(\alpha)} \left(n_k{}^{(\alpha)}\right)^2 = \frac{\rho^*}{3} \qquad \text{for } k = 1,..,3 \tag{3}$$

where $c^{(\alpha)} = \Omega_{UC}{}^{(\alpha)} / \Omega_{UC}$ is the volume fraction of plates (α) in a plate-lattice.

Ω_{UC} is the total volume of the hybrid unit cell.

20 ${\Omega_{UC}}^{(\alpha)}$ is the volume of plates (α).

21 UC denotes the group of plates contained in the unit cell.

22 $\boldsymbol{n}^{(\alpha)}$ is the unit vector along the thickness direction of plates (α).

23 $\rho^* = \rho/\rho_s = \sum_{\alpha \in UC} c^{(\alpha)}$ is the relative density of the plate-lattice.

24 ρ denotes the density of plate-lattice.

25 ρ_s is the density of the basis material.

26 These three topological constraints are applied to simple cubic (SC), face-centered cubic (FCC)
27 and body-centered cubic (BCC) plate-lattices which exhibit cubic symmetry [1]. Due to the cubic
28 symmetry, constraints (1) and (3) are automatically satisfied for all the three plate lattices considered.
29 Applying constraint (2) to the elementary plate-lattices gives

$$\sum_{\alpha \in SC} c^{(\alpha)} \left({n_k}^{(\alpha)}\right)^4 = \frac{C_{SC}}{3} \tag{4}$$

$$\sum_{\alpha \in FCC} c^{(\alpha)} \left({n_k}^{(\alpha)}\right)^4 = \frac{C_{FCC}}{9} \tag{5}$$

$$\sum_{\alpha \in BCC} c^{(\alpha)} \left({n_k}^{(\alpha)}\right)^4 = \frac{C_{BCC}}{6} \tag{6}$$

30 Where, C_{SC}, C_{FCC} and C_{BCC} are the volume fractions of SC, FCC and BCC lattices, respectively.

31 Using (4), (5) and (6) in constraint (2) gives the following topology constraint for achieving elastic
32 isotropy in a hybrid structure of SC-, BCC- and FCC-lattices.

$$\frac{C_{SC}}{3} + \frac{C_{FCC}}{9} + \frac{C_{BCC}}{6} = \frac{\rho^*}{5} \tag{7}$$

33 For a hybrid structure of SC- and FCC-lattices, the above criterion is satisfied when $C_{FCC} = \frac{3}{5}\rho^*$
34 which leads to elastic-isotropy of a hybrid structure of SC and FCC lattices with a volume fraction of 40%

and 60%, respectively. In the case of a hybrid structure of SC and BCC lattices, we obtain $C_{BCC} = \frac{4}{5}\rho^*$ to have elastic-isotropy. This indicates that the hybrid structure with SC and BCC lattices will have elastic isotropy if the volume fraction of SC is 20% and BCC is 80%. For a hybrid structure of SC, FCC and BCC lattices, an infinite number of solutions for equation (7) exist. In this study we use 30%, 60% and 40% volume fraction of SC, FCC and BCC plate-lattices as done by Tancogne-Dejean et. al. [1].

S1.2. Additive manufacturing of plate-lattice specimens

Plate-lattice specimens were fabricated using slide and separate™ (SAS™) 3D printing technology employing a PRO2-ASIGA desktop 3D printer [2]. The process parameters employed for fabricating the plate-lattice samples are summarized in *Table S1*. In this study, all samples were printed using PlasGRAY™ photopolymer whose physical and mechanical properties are listed in *Table S2* [3]. PlasGRAY™ resins are liquid-state chemicals that can be cured by exposing to UV-light. By solidifying successive deposits of the resin beside each other the plate-lattice structures were fabricated. Asiga Composer™ software was employed to prepare the CAD model for the printing process by adding necessary support structures. A slice thickness of 0.070 mm was maintained to achieve high-resolution fabrication.

Table S1: Process parameters for 3D-printing of the plate-lattices

Properties	Standard	Unit
Light Intensity	5.67	mW/cm^2
Exposure Time	9.54	S
Slice Thickness	0.07	mm
Heater Temperature	35	ºC
Separation Velocity	5	mm/s
Separation Distance	14	mm

The build chamber was maintained at a temperature of 35 °C to control the viscosity, reactivity and solidification process of the photopolymer. The specimens fabricated on the printer were removed from the

platform and the resin residue remaining on the fabricated specimens were removed by washing using isopropanol. To achieve full strength, the printed specimens were completely cured by exposing them to ultraviolet light for a time duration of 6 minutes.

Table S2: Physical and mechanical properties of PlasGRAY™ [3].

Properties	**Standard**	**Unit**
Color	Grey	-
Tensile Strength	51.1	MPa
Elongation at break	6.58	%
Flexural strength	86.8	MPa
Flexural modulus	1910	MPa
Hardness (Shore D)	82	Shore D
Viscosity	343	mPa s
Glass transition temperature	84	°C
Izod Notched-Impact	4.97	kJ/m²
Density	1.18	g/cm³

The model under fabrication is moved downwards into a tray of photopolymer resin to one layer thickness above the bottom of the tray. The bottom of the tray is made from a transparent Teflon film which will be deflected downwards as the model approaches it. A slider plate moves below the tray film, lifts its level and squeezes out surplus resin. A cross-sectional image of the sample being fabricated is projected onto the bottom of the tray film, initiating resin to solidify in the shape of the image. Then, the model is lifted out of the tray to detach it from the tray film. This process is repeated until the plate-lattice structure is built completely.

All dimensions were chosen by considering the build-envelope of our 3D printer (Asiga Pro2). Moreover, to avoid producibility constraints, the thickness of the ligaments are kept above 200 µm for the lowest relative density chosen (25%), which is way larger than the resolution of the 3D printer. We could

not print geometric features below 200 µm without holes or cracks in the structures due to the forces acting on the structure during digital light processing.

The hybrid SC-BCC-FCC was identified as the limiting structure, due to its large number of thin features, compared to elementary or other hybrid structures considered here. The unit cell was therefore scaled up to 20 mm in order to avoid producibility constraints. This led to a structure size 40 mm by 40 mm by 40 mm or 2x2x2 unit cells. Choosing this configuration of unit cells will unavoidably include edge effects. Analysis of edge effects is left to subsequent study. However, keeping this configuration constant for all tests, makes all results comparable and the general nature of the performance assessable.

From application view point, we suggest reducing the unit cell size to achieve a homogenous metamaterial, which can compete with foam-like structures. Previous studies [1] have shown, that lattice structures can be manufactured in much smaller unit cell sizes of 66 µm for a relative density of 30%.

The main interest behind comparing the constant thickness and constant density (relative density 35%) specimens is to qualitatively examine how the thickness distribution of different elementary structures influences the deformation profile pertinent to the energy absorbing mechanism. To simplify, we chose the structure with 35% relative density to compare, instead of comparing with structures of all available and tested relative densities. That way we have 2 structures (BCC and FCC) which are almost identical, only the hybrid and SC had to be adjusted significantly. On average that's the best choice for comparison.

Holes were introduced into all individual plate segments for the ease of fabrication (diameter 1 mm). They are necessary, in order to remove trapped and unsolidified resin after the manufacturing process, using isopropyl alcohol. Compared to the overall volume of the plates, they are negligible and don't have seem to affect the damage behaviour.

S1.3. Low-velocity impact tests

For measuring the energy absorption characteristics of plate-lattice samples, during low energy impact events, accurate measurement of the impactor velocity is essential. In this study, the velocity was measured by an optical laser measurement system where the distance travelled by the impactor between two photo-sensors was calculated according to the principle of triangulation [4, 5]. In order to measure the impactor velocity during the whole impact event, a laser beam is reflected back from the bottom surface of the impactor head. The receiving signal of the laser produces an output voltage proportional to the measured

distance. In the data acquisition system, the signal is then transformed to corresponding displacement, velocity and energy.

A dynamic load cell with a maximum load capacity of 30 kN with less sensitivity to structural vibrations was employed to measure the contact force during the impact events. The quartz element in the dynamic load cell generates an electric charge proportional to the applied impact force during the impact event. This electric charge is then fed into the DAQ system through a charge amplifier. Using the force-time response, it is possible to estimate the absorbed energy and displacement with respect to time applying Newton's 2nd law as

$$\delta(t) = \delta_i + v_i t + \frac{gt^2}{2} - \int_0^t \left[\int_0^{t'} \frac{F(t'')}{m} dt' \right] dt$$

$$E_a(t) = \frac{1}{2} m \left[{v_i}^2 - {v_f}^2(t) \right] + mg\delta(t)$$

Where, δ is the impactor displacement, δ_i is the reference position, v_i is the initial impact velocity, m is the impactor mass, F is the contact force and $E_a(t)$ is the absorbed energy at time t.

S2. Results and discussion

S2.1. Effect of the impact energy

The energy-time histories of different plate-lattice specimens at various impact energy levels are depicted in *Figure S1*. With increasing impact energy, the response of all specimens (excluding SC-BCC-FCC) depicted different energy-time trends. It can be observed that, for the BCC specimens, the energy-time curve raised linearly up to 13.78 J of dissipated energy (*Figure S1 (a)*), where the specimens completely ruptured (brittle fracture- *Figure 7*). For the case of SC and FCC specimens subjected to an impact energy of 20 J, *Figure S1* the specimens showed an elastic rebound phase, suggesting that the impact energy was not large enough to induce damage in the specimens. Moreover, the experimental curves of SC-BCC and SC-FCC specimens impacted at 20 J showed an incomplete rebound phase with some minor damages.

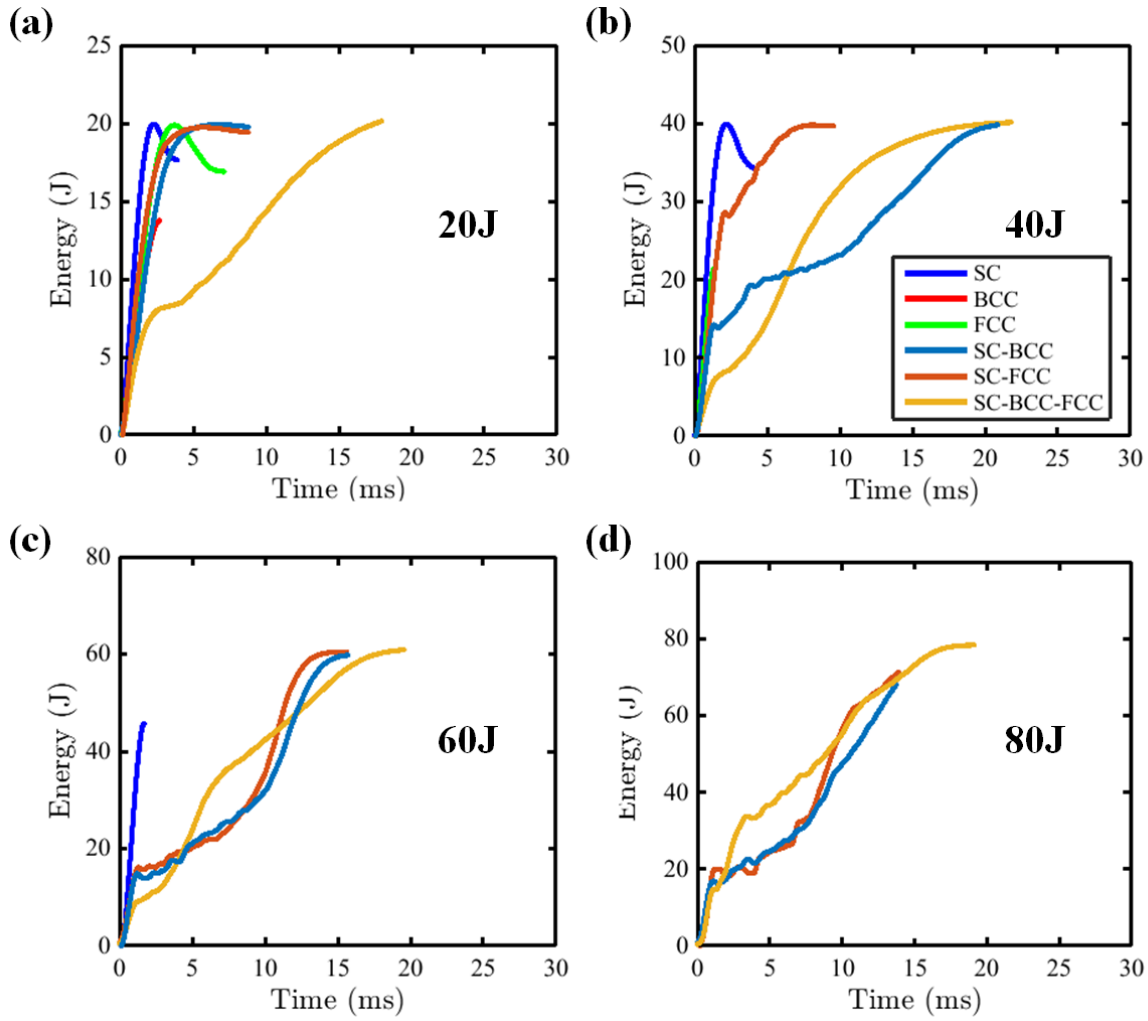

Figure S1: Energy vs. time histories of different plate-lattice specimens tested at different impact energies: (a) 20 J, (b) 40 J, (c) 60 J and (d) 80 J.

For the case of SC-BCC-FCC specimens, after the initial plateau region was reached, the energy-time history increased following almost a gradual and linear trend. It can be inferred from the experimental curves that, at all the impact energy levels, SC-BCC-FCC specimens had a long oscillation region and encountered long contact duration before reaching the ultimate failure.

Table S3: Liner stiffness of different plate-lattice specimens at impact energy 20 J

Specimens	Stiffness (N/mm)
SC	6579.6
BCC	3438.8
FCC	3288.3
SC-BCC	4645.5
SC-FCC	5198.2
SC-BCC-FCC	5193.2

S2.2 Constant plate thickness vs. constant relative density

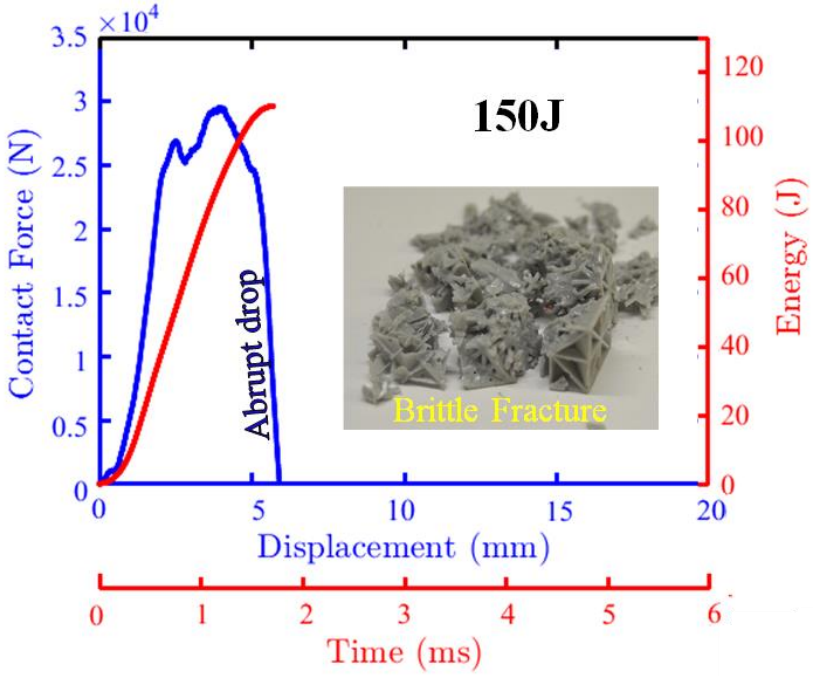

Figure S2: Contact force-displacement, energy-time and damage profile (inset) of SC-BCC-FCC specimen with constant plate thickness at 150 J.

S2.3 Effect of relative density

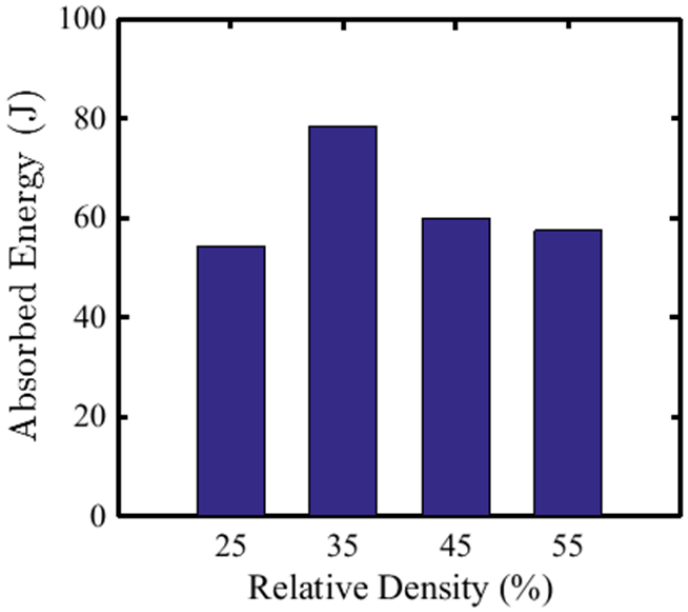

Figure S3: Absorbed energy vs. relative density bar chart of SC-BCC-FCC specimens for various relative densities under impact energy of 80 J.

S2.4 Effect of multiple impacts

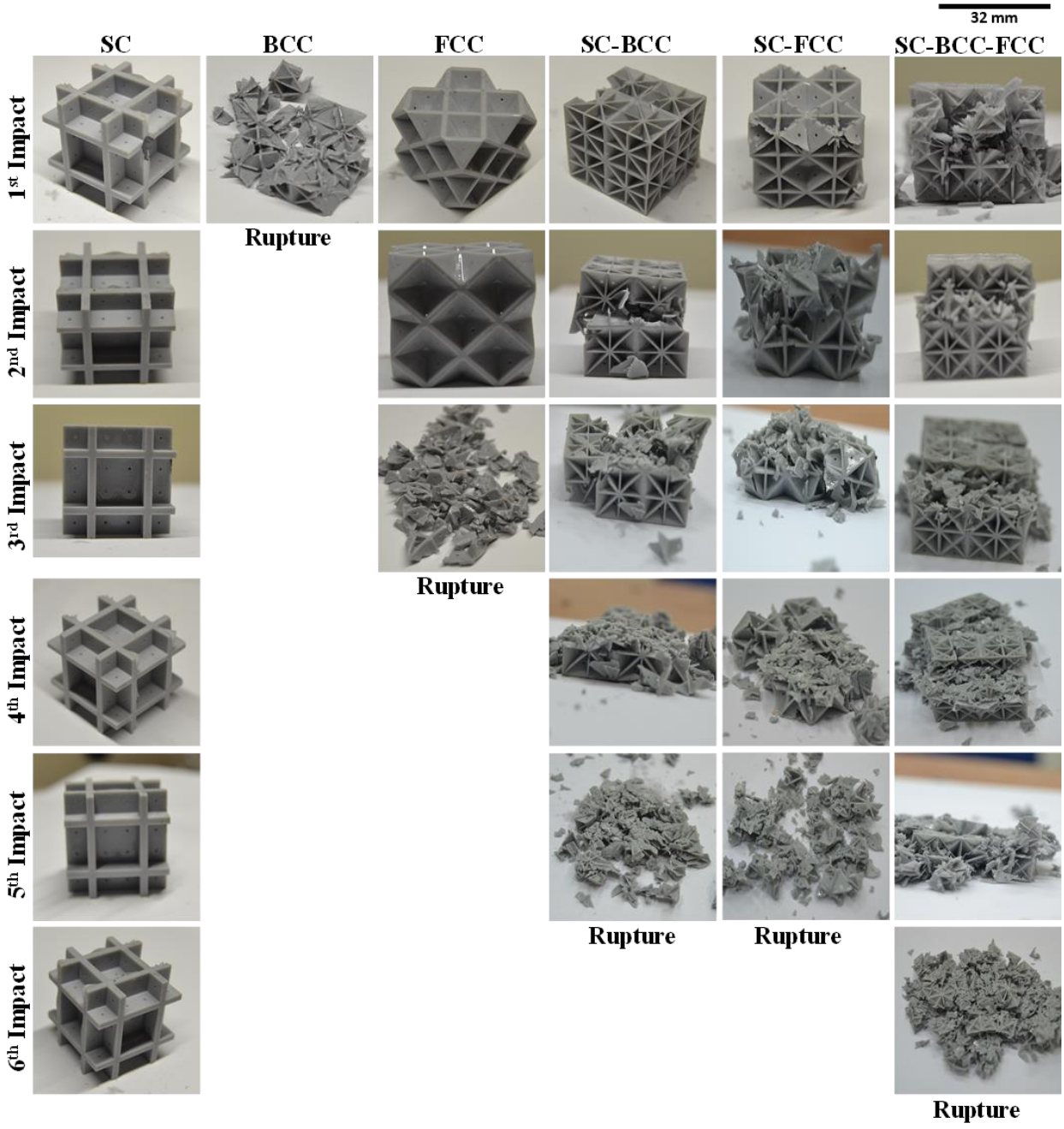

Figure S4: Post-test photographs of various plate-lattice specimens subjected to multiple impacts at 20 J.

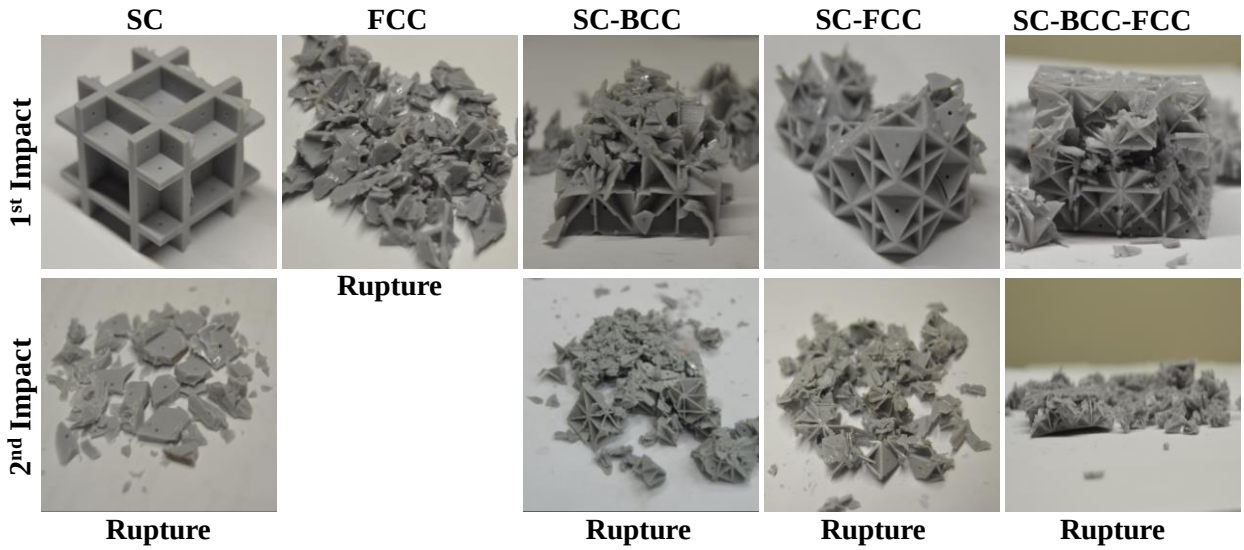

158

159 *Figure* S5: Post-test photographs of various plate-lattice specimens subjected to multiple impacts at an

160 impact energy of 40 J.

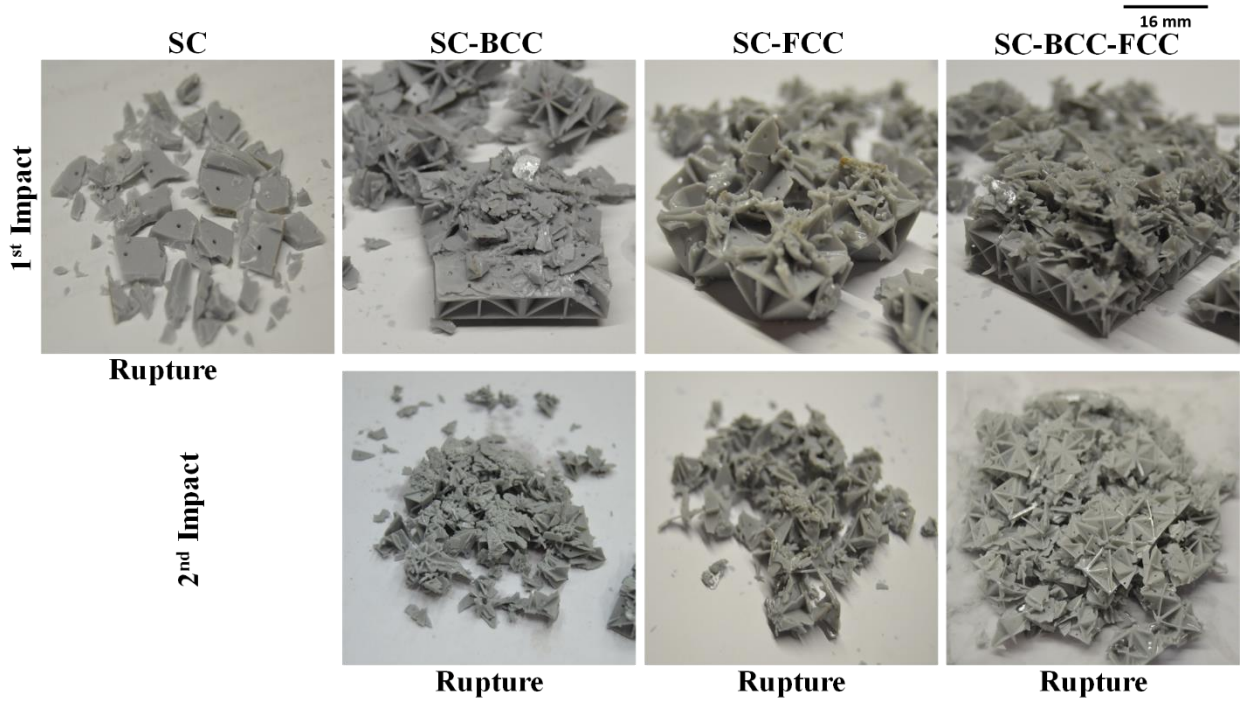

161

162 *Figure* S6 Post-test photographs of various plate-lattice specimens subjected to multiple impacts at an

163 impact energy of 60 J.

S2.5 Effect of impact angle

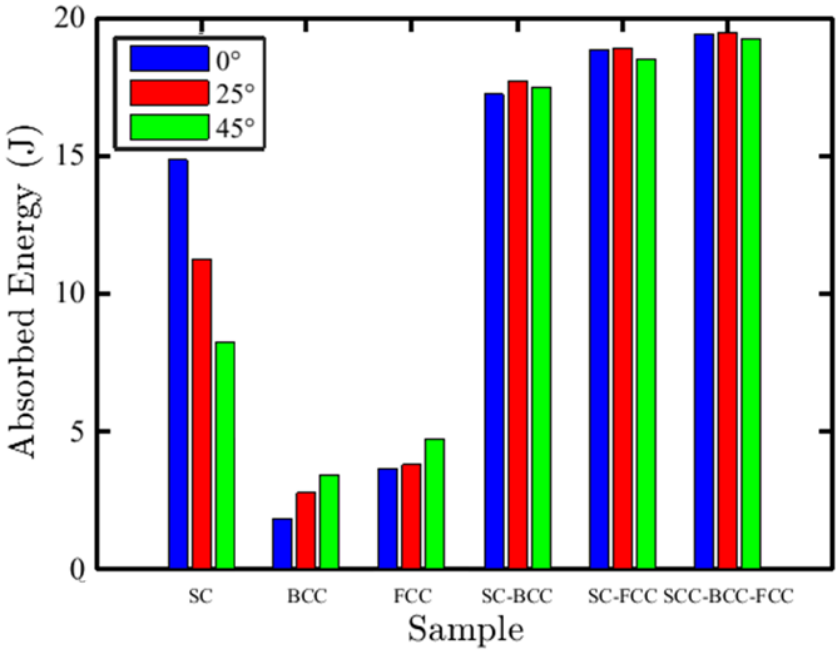

Figure S7: Absorbed energy of various plate-lattice specimens for 0º, 25º and 45º tested angles.

References:

1. Tancogne-Dejean, Thomas, Marianna Diamantopoulou, Maysam B. Gorji, Colin Bonatti, and Dirk Mohr. "3D Plate-Lattices: An Emerging Class of Low-Density Metamaterial Exhibiting Optimal Isotropic Stiffness." Advanced Materials 30, no. 45 (2018): 1803334.
2. https://www.asiga.com/products/printers/pro2/
3. https://dl.airtable.com/N8cuSP8KTLODEVqwZFde_PlasGRAY_us_en.pdf
4. R. Juntikka, S. Hallström, Weight-balanced drop test method for characterization of dynamic properties of cellular materials, Int. J. Impact Eng. 30 (2004) 541–554.
5. P. Feraboli, Some Recommendations for characterization of composite panels by means of drop tower impact testing, J. Aircr. 43 (2006) 1710–1718.
6. Sarasini, F., et al., Drop-weight impact behavior of woven hybrid basalt–carbon/epoxy composites. Composites Part B: Engineering, 2014. **59**: p. 204-220.